

## Article

# Structural and Optical Characterization of Silica Nanospheres Embedded with Monodisperse CeO<sub>2</sub>-Eu<sup>3+</sup> Nanocrystals

Corina Secu <sup>1</sup>, Cristina Bartha <sup>1</sup> , Elena Matei <sup>1</sup> , Cristian Radu <sup>1,2</sup> and Mihail Secu <sup>1,\*</sup>

<sup>1</sup> National Institute of Materials Physics, Atomistilor 405A, 077125 Magurele, Romania; cesecu@infim.ro (C.S.); cristina.bartha@infim.ro (C.B.); elena.matei@infim.ro (E.M.); cristian.radu@infim.ro (C.R.)

<sup>2</sup> Faculty of Physics, University of Bucharest, Atomistilor 405, 077125 Magurele, Romania

\* Correspondence: msecu@infim.ro

**Abstract:** Luminescent nanocrystals embedded into silica microspheres were shown to be useful for silica labeling for biological applications, ensuring mechanical and chemical stability, nontoxicity, biocompatibility and optical properties. We used sol-gel technology to prepare silica nanospheres embedded with fluorescent and magnetic Eu<sup>3+</sup> (1 mol%)-doped CeO<sub>2</sub> nanocrystals. The X-ray diffraction pattern analysis and transmission electron microscopy investigations showed CeO<sub>2</sub>:Eu<sup>3+</sup> (1 mol%) nanocrystals of about 9 nm size and Ce<sup>3+</sup> ions substitution by the Eu<sup>3+</sup> ions; the nanocrystals dispersed inside the nanosized silica spheres of about 400 nm diameters. The photoluminescence spectra recorded under UV-light excitation showed Eu<sup>3+</sup> ions luminescence peaks (<sup>5</sup>D<sub>0</sub>-<sup>7</sup>F<sub>J</sub>, J = 0-4) accompanied by a weaker 425 nm luminescence due to the silica matrix; the quantum yield was 0.14. The weak hysteresis loop and magnetization curves recorded up to 20,000 Oe showed dominantly paramagnetic behavior associated with the silica matrix; a slight opening of the hysteresis loop to a very small magnetic field (about 0.005 Oe) was due to the presence of the two rare earth ions. The photonic crystal properties of SiO<sub>2</sub>-CeO<sub>2</sub>:Eu<sup>3+</sup> (1 mol%) silica nanospheres deposited as films on quartz plates were revealed by the two weak attenuation peaks at 420 and 500 nm and were associated with the reflection from different planes. The SiO<sub>2</sub>-CeO<sub>2</sub>:Eu<sup>3+</sup> (1 mol%) nanospheres are attractive potential candidates for photonics-related applications or for multifunctional bio-labels by combining the luminescence and magnetic properties of the nanocrystals.

**Keywords:** CeO<sub>2</sub>; europium; silica spheres; nanocrystals; electron microscopy; luminescence



**Citation:** Secu, C.; Bartha, C.; Matei, E.; Radu, C.; Secu, M. Structural and Optical Characterization of Silica Nanospheres Embedded with Monodisperse CeO<sub>2</sub>-Eu<sup>3+</sup> Nanocrystals. *Magnetochemistry* **2022**, *8*, 22. <https://doi.org/10.3390/magnetochemistry8020022>

Academic Editor: Fabrice Pointillart

Received: 14 January 2022

Accepted: 1 February 2022

Published: 4 February 2022

**Publisher's Note:** MDPI stays neutral with regard to jurisdictional claims in published maps and institutional affiliations.



**Copyright:** © 2022 by the authors. Licensee MDPI, Basel, Switzerland. This article is an open access article distributed under the terms and conditions of the Creative Commons Attribution (CC BY) license (<https://creativecommons.org/licenses/by/4.0/>).

## 1. Introduction

Rare-earth-doped nanomaterials are widely studied due to characteristics related to the presence of unpaired electrons in the inner 4f sub-shell: fluorescence, downconversion, upconversion, persistent phosphorescence and also magnetic properties, with applications spanning from laser optoelectronics, optical amplifiers, lasers, up-converters to biosensing, biology carrier applications and multifunctional imaging ([1,2] and references therein). In order to maintain their functionalities for practical applications, it is necessary to isolate them with a thin SiO<sub>2</sub> layer around the nanocrystalline core and that results in a core-shell composite. The coating of the nanocrystals with a thin SiO<sub>2</sub> shell provides several advantages such as: protection against oxidation and agglomeration, increase in the mechanical stability, and enabling dispersion in various aqueous solvents. Furthermore, the surface of silica particles can be chemically modified to link bioconjugates. As the silica can be easily made controllable in spherical morphology from nano-to micrometer size [3], a novel approach is to embed the nano-phosphors in a transparent inert silica matrix [4-7]. Fluorescent microspheres can be produced by the incorporation of luminescent nanocrystals into the bigger silica microspheres and have been demonstrated to be useful for silica labeling in a variety of biological or phosphor related applications [4-6]. Whatever the path used, the grains with core-shell architecture can combine diverse functionalities into a

single hybrid composite with improved or new physical properties compared with those of each component.

Ceria ( $\text{CeO}_2$ ) is an insulating pale-yellow oxide with a cubic fluorite structure (space group  $Fm\bar{3}m$ ) and is a widely studied material with various applications, the main one being related to oxidative catalysis [8]. Rare-earth-doped  $\text{CeO}_2$  has attracted great interest for various applications including high oxygen storage capacity, electrolytes for intermediate-temperature or electrolyte and anode material [9]. Most of the previous studies were related to the  $\text{CeO}_2$  material properties' improvement, but doping is accompanied by unique optical features which originate from their  $4f$ -electronic configuration [10]. In particular, regarding photoluminescence properties induced by rare-earth doping for  $\text{Eu}^{3+}$ -doped  $\text{CeO}_2$  nanoparticles, the mechanism has been extensively investigated [11–14]. Great efforts have been made to understand the relationship between morphology, dimensions, surface chemistries, crystalline defects and fluorescent properties [14]; all of them showed a high influence on the  $\text{Eu}^{3+}$  emission [14]. On the other hand, the magnetic properties shown by  $\text{CeO}_2$  nanoparticles have been widely investigated in terms of the influence of the morphology, defect structure of the oxide and the influence of the impurities [15–18]. As pure  $\text{CeO}_2$  is composed of nominally closed-shell ions (with no unpaired electrons), it might be expected to present an independent orbital diamagnetism, but well-crystallized stoichiometric  $\text{CeO}_2$  show a weakly paramagnetic behavior associated with oxygen vacancies or pentavalent substitutions in the structure ([15] and references therein). Moreover, rare-earth-doped  $\text{CeO}_2$  powders show room temperature ferromagnetism (RE = Nd, Sm) or paramagnetism (RE = Gd, Tb, Er, Dy) associated with oxygen vacancies and the formation of fluorite crystal structure [9,17].

The aim of the present study was to prepare silica nanospheres embedded with  $\text{Eu}^{3+}$  (1 mol%)-doped  $\text{CeO}_2$  nanocrystals in order to combine the magnetic and optical functionalities into a single hybrid composite and to perform a structural, morphological investigation by using X-ray diffraction and electron microscopy techniques. Then, the magnetic and optical properties such as photoluminescence, quantum efficiency and optical absorption were investigated and discussed.

## 2. Materials and Methods

### 2.1. Samples Preparation

For the preparation of silica nanospheres embedded with  $\text{Eu}^{3+}$  (1 mol%)-doped  $\text{CeO}_2$  nanocrystals we used a two-step approach. Firstly, we synthesized  $\text{Eu}^{3+}$  (1 mol%)-doped  $\text{CeO}_2$  nanocrystals by using polyvinyl-pyrrolidone (PVP) solution route [19] and using cerium (III) acetate hydrate (Sigma-Aldrich, Saint Louis, MO, USA, 99.9%), europium (III) acetate hydrate (Sigma-Aldrich, Saint Louis, MO, USA, 99.9 and polyvinyl pyrrolidone (PVP) ( $M_n = 1,300,000$ , Sigma-Aldrich, Saint Louis, MO, USA) as the starting chemicals. In the first step, a water solution was made by 1.5 g of PVP dissolved in 100 mL of de-ionized water under vigorous stir at 27 °C for 30 min. A powder mixture of 0.99 g of cerium (III) acetate hydrate and 0.01 g europium (III) acetate hydrate was added to the PVP solution under vigorous stir at 60 °C for 30 min until a well-dissolved solution was obtained. Then, the water solution was evaporated by heating in a water bath at 60 °C, and the resulting solid precursor was dried in an oven at 100 °C. Finally, the dried precursor was calcined in open atmosphere at 500 °C for 2 h.

In the second step, we proceeded with the preparation of the  $\text{Eu}^{3+}$  (1 mol%)-doped  $\text{CeO}_2$  nanocrystalline powders embedded in silica spheres (4% wt,  $\text{CeO}_2:\text{Eu}/\text{SiO}_2$ ) according to the procedure described in ref [15]. The  $\text{CeO}_2:\text{Eu}$  (1 mol%) nanocrystalline powder (0.0168 g) was ultrasonically dispersed in 21 mL of ethanol ( $\geq 99.8\%$ , Sigma-Aldrich, Saint Louis, MO, USA). Then, to the mixture was added 1.55 mL of TEOS (99.9%, Alfa-Aesar, Heysham, Lancashire, UK) and 5.5 mL of aqueous ammonia solution (25%; Merck, Darmstadt, Germany), and a silica sol was produced. The sol solution was stirred at room temperature for 2 h, and a silica powder was formed at the bottom of the vessel; the powder was filtered, dried and used for the measurements.

## 2.2. Samples Characterization

For the structural analysis of the samples, we used a BRUKER D8 ADVANCE (Billerica, MA, USA) type X-ray diffractometer in focusing geometry, with a copper target X-ray tube and a LynxEye one-dimensional detector. The XRD pattern was recorded in the 20 to 80° range with 0.05° step and 3 s integration time. The crystalline phase analysis and crystal structure refinement was made by using the Rietveld analysis approach and a dedicated software (MAUD, Springfield, MA, USA) [20,21] with the starting parameters from PDF 04-015-2673 (CeO<sub>2</sub>) files from the ICDD Powder Diffraction Files database [22]. For the morphological analysis by scanning electron microscopy (SEM), we used an EVO 50 XVP and Merlin Compact equipment from Zeiss (Jena, Germany). Transmission electron microscopy (TEM) analysis of the samples was performed by using the ARM200F electron microscope equipped with an energy-dispersive X-ray spectrometer (EDS); the accelerating voltage of the electron beam was 200 kV. The optical characterization of the samples was performed by using photoluminescence and absorption spectroscopy. The photoluminescence and excitation spectra were recorded at room temperature by using a FluoroMax 4P spectrophotometer (HORIBA Jobin Yvon, Kyoto, Japan); for the chromaticity and quantum efficiency analysis, we used the QuantaPhy accessory. Optical absorption spectra were performed on thin-film samples deposited by the spin-coating technique on quartz substrates and by using a Varian Cary 4000 UV–Vis spectrophotometer, (Agilent Technologies Inc. Santa-Clara, CA, USA) in the 250 to 800 nm range with 1 nm step. The magnetic properties were investigated with a Superconducting Quantum Interference Device (SQUID) from Quantum Design. Both curves, the hysteresis loop and magnetization versus applied magnetic fields were acquired at room temperature under a magnetic field up to 50,000 Oe.

## 3. Results

### 3.1. Structural and Morphological Characterization

In Figure 1, the XRD pattern of Eu<sup>3+</sup> (1%)-doped CeO<sub>2</sub> nanocrystalline powder calcinated for 2 h at 500 °C and the results of the Rietveld refinement are presented. The analysis results from Tables 1 and 2 only show the presence of cerium europium oxide crystalline phase without any additional ones, with the lattice parameters very close to those from the ICDD database (PDF 04-015-2673) [22]; the nanocrystallite's size agrees very well with TEM microscopy data (see below). Structural analysis of undoped CeO<sub>2</sub> nanocrystals prepared by using the same PVP solution route [19] is shown for the lattice parameter  $a = 0.5394 \pm 0.0002$  nm and the nanocrystals with sizes of 11.6 nm. Therefore, the PVP solution method [19] and processing conditions ensured the substitutional incorporation of Eu<sup>3+</sup> dopant ions in the CeO<sub>2</sub> crystalline matrix accompanied by a weak lattice expansion and without oxygen-related defects, vacancies or additional parasite phases that might influence the magnetism ([15] and references therein). Hence, compared to the other synthesis methods, the PVP solution method is useful to investigate the Eu<sup>3+</sup>-ions' dopant effects on magnetic properties (without any other interferences) by correlation to the structural ones.

The morphology and structure analysis of the CeO<sub>2</sub>:Eu<sup>3+</sup> nanocrystalline powder by using electron microscopy TEM are presented in Figure 2. The TEM image shows agglomerated nanoparticles about 5–10 nm in size, and the selected-area electron diffraction (SAED) pattern shows spotty ring patterns, confirming the CeO<sub>2</sub> crystalline structure with  $a = 0.541$  nm.

The SEM images of the SiO<sub>2</sub>-CeO<sub>2</sub>:Eu<sup>3+</sup> nanospheres (Figure 3) showed a relatively uniform distribution of nanospheres about 350 nm in size. Low-magnification TEM imaging evidenced spherical silica particles of about 300–400 nm in size containing dispersed CeO<sub>2</sub> nanocrystals mostly in the central region, as can be seen in Figure 4a; some of the spheres seem to show CeO<sub>2</sub> nanocrystals on their surface, as was revealed by high-magnification TEM imaging (Figure 4b).

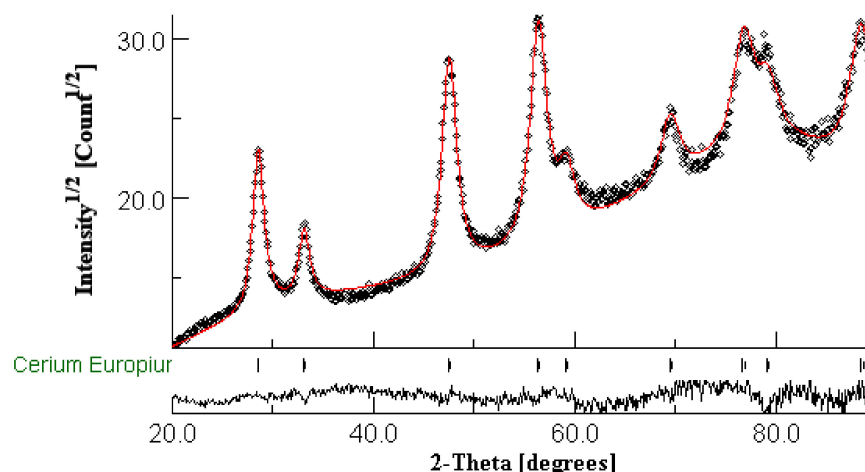


**Figure 1.** XRD pattern (black curve) and Rietveld refinement plot (red curve) of  $\text{Eu}^{3+}$ (1%)-doped  $\text{CeO}_2$  nanocrystalline powder calcinated at  $500\text{ }^\circ\text{C}$ ; the lower trace represents the difference curve between observed and calculated patterns.

**Table 1.** The Rietveld refinement analysis results for  $\text{Eu}^{3+}$ (1%)-doped  $\text{CeO}_2$  nanocrystalline powders calcinated at  $500\text{ }^\circ\text{C}$ .

Crystalline Phase	$\text{Ce}_{0.95}\text{Eu}_{0.05}\text{O}_{1.975}$ (Cerium Europium Oxide)	R Factors (%)
Weight fraction (%)	$100 \pm 0.0$	
Crystal size (nm)	$9.0538 \pm 2.184$	
Crystal system	Cubic	
Space group	Fm-3 m	$R_{\text{wp}} (\%) = 4.3656$
Unit cell theoretic ( $\text{\AA}$ ) (PDF 04-015-2673)	5.394	$R_{\text{b}} (\%) = 3.417$
Unit cell calculated ( $\text{\AA}$ )	$5.409 \pm 0.041$	$R_{\text{exp}} = 2.305$
Cell_angle_alpha	$90^\circ$	$\chi^2 = 1.893$
Cell_angle_gamma	$90^\circ$	
Cell Volume ( $\text{\AA}^3$ )	156.94	
Microstrain	$3.2 \times 10^{-6} \pm 0.001$	

**Table 2.** Atomic site occupancy for  $\text{Eu}^{3+}$ (1%)-doped  $\text{CeO}_2$  nanocrystals calcinated at  $500\text{ }^\circ\text{C}$ .

Atoms	$\text{Ce}_{0.95}\text{Eu}_{0.05}\text{O}_{1.975}$ (Calc.)			$\text{Ce}_{0.95}\text{Eu}_{0.05}\text{O}_{1.975}$ (Theor.)			Wyckoff Site	Atom Site Occupancy (Theor/Calc)
	x	y	z	x	y	z		
Ce1	0.0	0.0	0.0	0.0	0.0	0.0	4a	0.95/0.8364(5)
Eu2	0.0	0.0	0.0	0.0	0.0	0.0	4a	0.05/0.0494(3)
O3	0.2498 (3)	0.2495 (2)	0.2499 (4)	0.25	0.25	0.25	8c	0.988/1.0228(6)

The nature and the dispersion of the nanoparticles inside the silica spheres were revealed by scanning transmission electron microscopy (STEM) images in dark field mode. They showed a central region consisting of elements with higher atomic numbers, as it appears brighter than the surrounding material, as it is the case of Ce atoms compared with Si. The STEM-EDS mapping images revealed the presence of  $\text{CeO}_2$  nanocrystals mainly in the core region of the sphere but also partially dispersed in the volume (Figure 5).

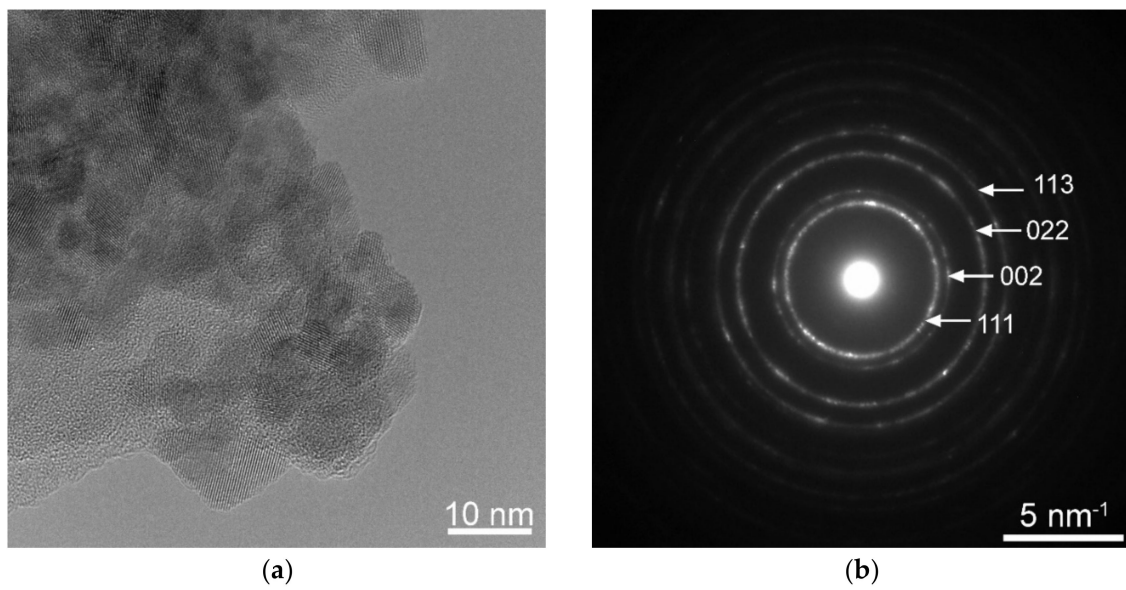


**Figure 2.** TEM microscopy showing  $\text{CeO}_2:\text{Eu}^{3+}$  nanoparticles (a) and the corresponding SAED where the Miller indices of the main diffraction spots are indicated (b).

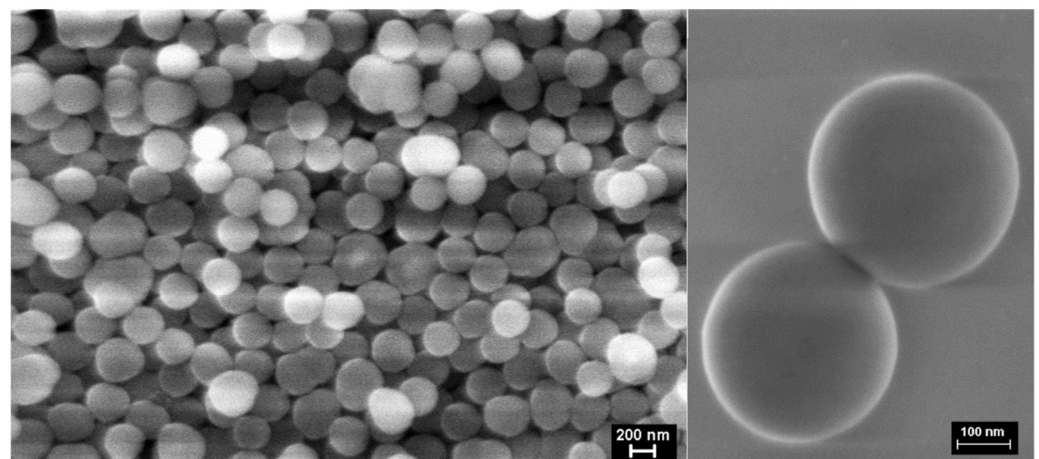


**Figure 3.** The SEM image of the silica  $\text{SiO}_2\text{-CeO}_2:\text{Eu}^{3+}$  nanospheres.

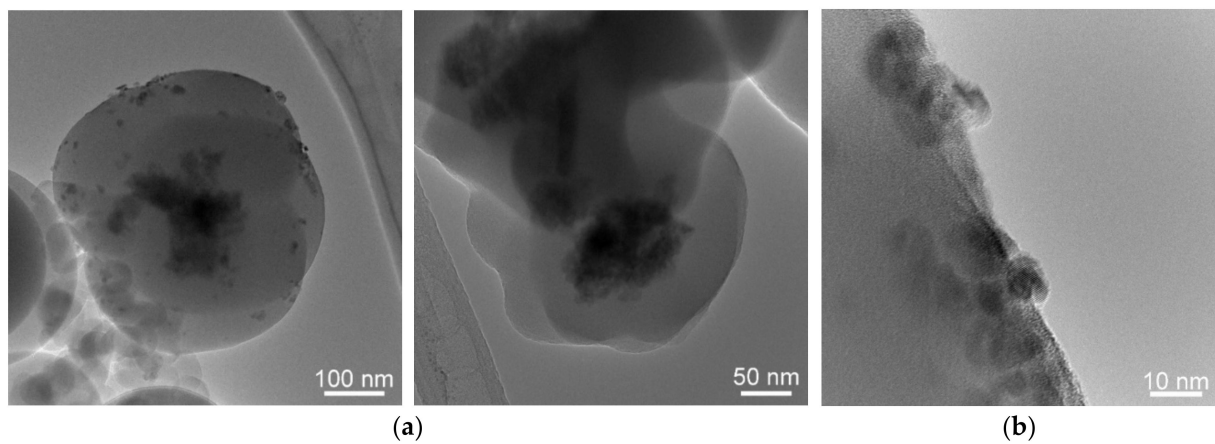


**Figure 4.** Low-magnification TEM images (a) and high-magnification TEM image (b) of silica  $\text{SiO}_2\text{-CeO}_2:\text{Eu}^{3+}$  nanospheres.

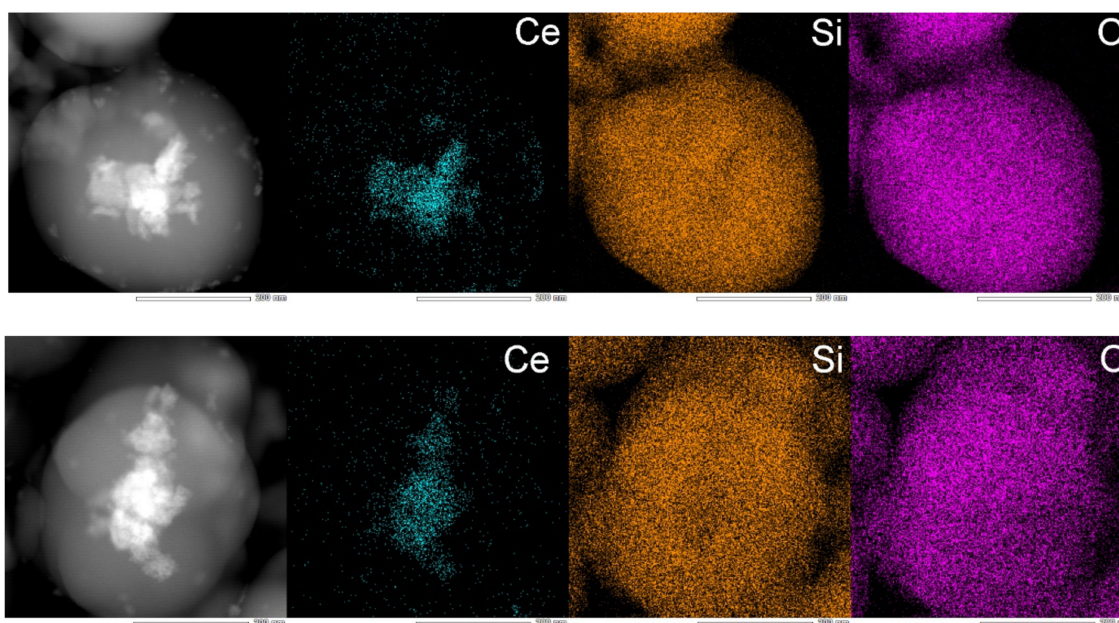


**Figure 5.** STEM images of  $\text{SiO}_2\text{-CeO}_2\text{:Eu}^{3+}$  silica nanospheres.

### 3.2. Optical Properties

The visual observation of a solution of  $\text{SiO}_2\text{-CeO}_2\text{:Eu}^{3+}$  (1 mol%) silica nanospheres solution (in ethanol) under 360 nm UV-light excitation showed a red-pink luminescence due to the  $\text{Eu}^{3+}$  luminescent ions (Figure 6).

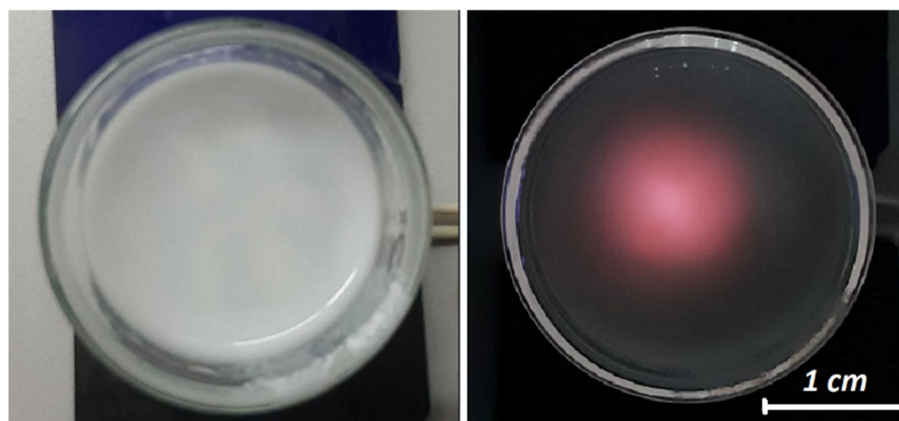


**Figure 6.** Optical images of  $\text{SiO}_2\text{-CeO}_2\text{:Eu}^{3+}$  silica nanospheres solution (in ethanol) under daylight (left) and 360 nm spotlight excitation (right).

### 3.3. Photoluminescence Properties

The photoluminescence and excitation spectra recorded on  $\text{SiO}_2\text{-CeO}_2\text{:Eu}^{3+}$  (1 mol%) silica nanospheres are depicted in Figure 7a. Under 345 nm excitation, the photoluminescence spectrum exhibited a sharp and intense emission at 590 nm, accompanied by a broad blue, weaker luminescence at about 425 nm assigned to the silica matrix. The 590 nm sharp emission peak is due to the  $^5\text{D}_0\text{-}^7\text{F}_1$  magnetic dipole transition of  $\text{Eu}^{3+}$  ions, while emission through the  $^5\text{D}_0\text{-}^7\text{F}_2$  electric dipole transition between 600 and 650 nm are very weak (Figure 7). According to the structural data analysis (Section 3.1) and for low dopant ions' concentration, the  $\text{Eu}^{3+}$  dopant ions substitute the high-symmetry octahedral  $\text{Ce}^{4+}$  sites within the  $\text{CeO}_2$  crystalline lattice [11,12], and therefore, the hypersensitive  $^5\text{D}_0\text{-}^7\text{F}_2$  electric dipole transition at 610 nm and 630 nm is suppressed. The single weak, sharp peak at 570 nm is due to the  $^5\text{D}_0\text{-}^7\text{F}_0$  transition and is consistent with a single  $\text{Eu}^{3+}$ -site in the

CeO<sub>2</sub> lattice [23]. The broad band peaking at 345 nm observed in the excitation spectrum of 590 nm luminescence is due to the charge transfer (CT) transition from O<sup>2-</sup> to Ce<sup>4+</sup> (not from the oxygen vacancy or from the CT of O<sup>2-</sup> to Eu<sup>3+</sup> [12]), and the subsequent energy transfer to excited 4f states of Eu<sup>3+</sup> ions followed by their radiative deexcitation. The location of the excitation peak agrees with the 340 nm band observed for 15 nm sized CeO<sub>2</sub>:Eu<sup>3+</sup> (1%) nanocrystals [12] and is shifted from the 373 nm band observed on CeO<sub>2</sub>:Eu<sup>3+</sup> microcrystalline phosphor powders [11]. The reasons for the shifts of the excitation spectra are supposed to be related to the nanosize influence on the band gap through the environmental factor, and was discussed in detail in refs. [12,24].

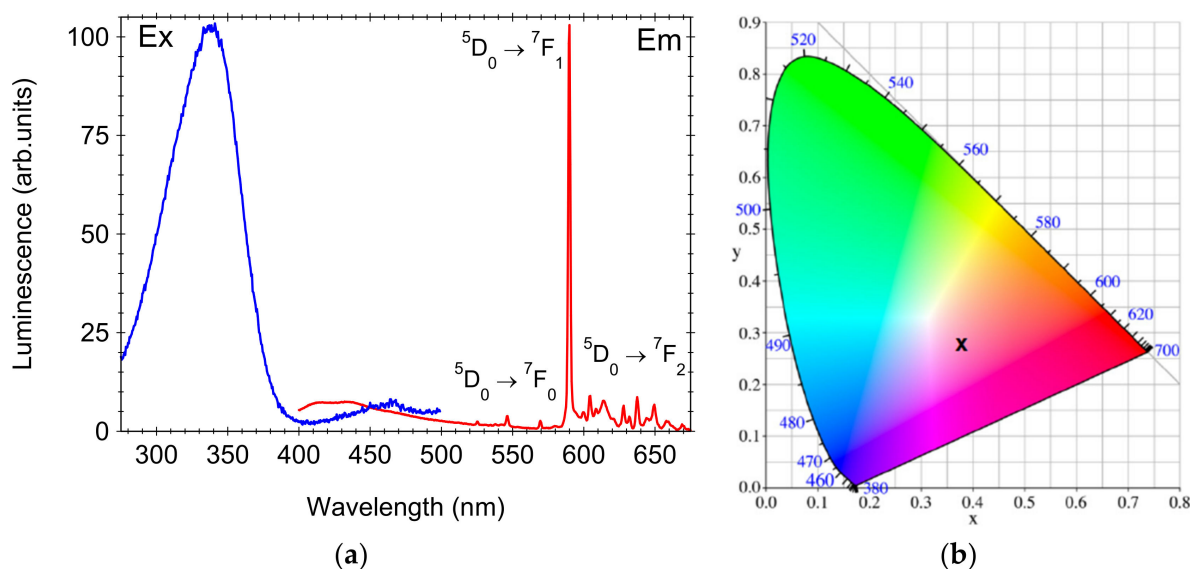


**Figure 7.** Photoluminescence and excitation spectra of SiO<sub>2</sub>-CeO<sub>2</sub>:Eu<sup>3+</sup> (1 mol%) silica nanospheres (a) and the chromaticity coordinates of the Commission Internationale de l’Eclairage (CIE) chromaticity diagram (b).

In Figure 7b, the Commission Internationale de l’Eclairage (CIE) chromaticity diagram of SiO<sub>2</sub>-CeO<sub>2</sub>:Eu<sup>3+</sup> nanocomposite spheres is shown. Under 345 nm UV excitation, the coordinates  $x = 0.37$  and  $y = 0.28$  were relatively close to the region of red Eu<sup>3+</sup> luminescence (Figure 7), and the photoluminescence quantum efficiency was about 14%. The high efficiency under 345 nm UV-light excitation was given by the CT transition from O<sup>2-</sup> to Ce<sup>4+</sup> followed by the energy transfer to the Eu<sup>3+</sup> excited states and then photoluminescence [25].

### 3.4. Optical Absorption

Finally, interesting features are revealed by the optical transmission spectra recorded on SiO<sub>2</sub>-CeO<sub>2</sub>:Eu<sup>3+</sup> (1 mol%) nanospheres deposited as thick films on quartz plates (Figure 8); the visual observation of iridescence might suggest photonic properties [26]. As expected, the spectra showed transparency in the whole visible and blue region down to 300 nm and strong absorption in the UV region due to the silica matrix. In addition, there are two weak attenuation peaks at 420 and 500 nm in the range expected for Bragg reflection from different planes [26,27] in the fcc structure, most probably (200) and (111) (Figure 8). The peaks position can be computed by the Bragg law at normal incidence and are dependent on the value fraction of the silica spheres in a close-packed structure and the refractive index of the silica spheres [27]. In the present case, their position is different from that reported at about 450 and 600 nm in [27], and they are very weak because of the poor packaging of the silica spheres (Figure 3), and the dispersion of the SiO<sub>2</sub>-CeO<sub>2</sub>:Eu<sup>3+</sup> (1%) nanospheres refractive index is different compared to silica spheres (due to the nanocrystals).

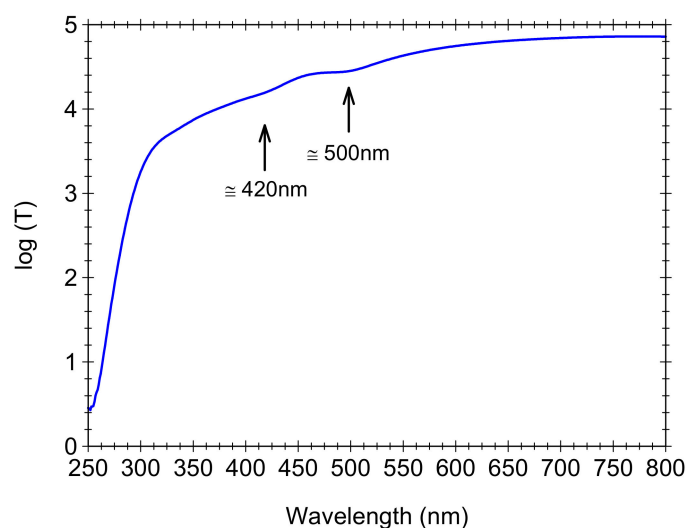


**Figure 8.** The logarithm of the transmission  $T$  vs. the wavelength for  $\text{SiO}_2\text{-CeO}_2\text{:Eu}^{3+}$  (1mol%) silica nanospheres deposited as thin films.

### 3.5. Magnetic Properties

The magnetic properties of the  $\text{SiO}_2\text{-CeO}_2\text{:Eu}^{3+}$  (1%) spheres are revealed by the magnetization vs. applied magnetic field dependence which indicates a diamagnetic behavior up to higher magnetic fields (Figure 9). In general, the magnetic properties of  $\text{CeO}_2$  are influenced by the morphology, defect structure and impurities [15–19] through the oxygen vacancies and structural defects. Moreover, it was shown that the  $\text{CeO}_2$  magnetic behavior is strongly influenced by the nanocrystals' dispersion in powders: the magnetism is reduced up to an order of magnitude and there is a characteristic length scale of the order of 100 nm for the magnetism to appear in  $\text{CeO}_2$  nanoparticle clusters [28]. In the present case, the diamagnetic behavior is dominantly given by the silica matrix, where the nanocrystals are incorporated and  $\text{CeO}_2$  magnetism is not observed. However, the presence of  $\text{CeO}_2\text{:Eu}^{3+}$  (1%) nanocrystals is revealed by a light open hysteresis loop observed at a very small magnetic field (about 0.005 Oe), which is due to the interaction between the two rare earths, Eu and Ce; the high number of 4f electrons causes an increase in the strength of the orbital couplings between the two ion sublattices.

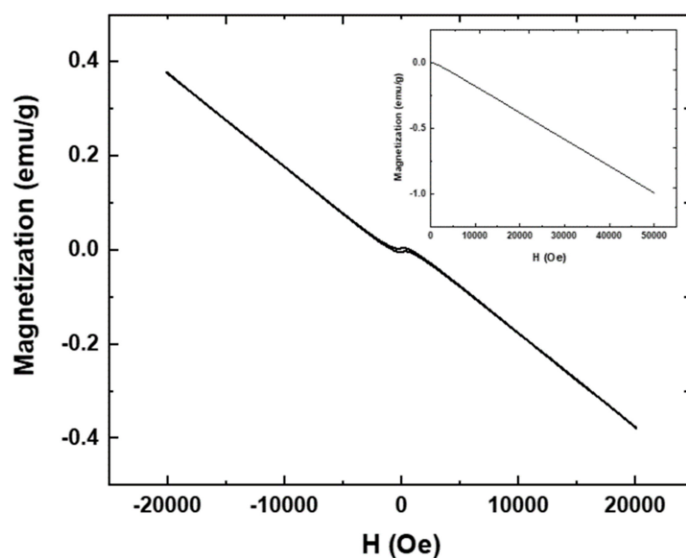


**Figure 9.** The magnetization vs. applied magnetic field dependence recorded at room temperature on  $\text{SiO}_2\text{-CeO}_2\text{:Eu}^{3+}$  silica nanospheres.

#### 4. Conclusions

Sol–gel technology was used to prepare monodisperse silica nanospheres embedded with  $\text{Eu}^{3+}$  (1%)-doped  $\text{CeO}_2$  nanocrystals. The electron microscopy images showed  $\text{CeO}_2$  nanocrystals dispersed within the silica nanospheres. The fluorescence properties related to the  $\text{Eu}^{3+}$  luminescent ions in the  $\text{CeO}_2$  crystalline matrix and paramagnetic properties due to the cerium ions; the interaction between the two ions was revealed by a slight opening of the hysteresis loop observed at a very small magnetic field. The photonic crystal properties of the silica nanospheres deposited as films were revealed by weak optical absorption dips in the visible range.

Hence, the  $\text{SiO}_2\text{-CeO}_2\text{:Eu}^{3+}$  (1 mol%) nanospheres structures can be used to host other high refractive index materials in order to obtain a full photonic band gap material. They are attractive potential candidates for photonics-related applications or for multifunctional bio-labels by combining the luminescence and magnetic properties of the nanocrystalline core, and the approach can be applied for other nanocomposites systems. However, further improvements to the optical properties and transparency through controlled deposition by using Langmuir Blodgett assembly, controlled evaporation or other techniques accompanied by a proper characterization of the magnetic behavior, i.e., the interaction between the ions, must be achieved.

**Author Contributions:** All the authors cooperated in the physical characterization and analysis of all the data: C.S. was involved in the sample preparation and XRD measurements; C.B. was responsible for the Rietveld refinement and magnetic measurements; M.S. was responsible for the optical properties (photoluminescence, efficiency and colorimetric analysis) and manuscript submission; E.M. was responsible with the morphological analysis by using scanning electron microscopy and C.R. was responsible for the morphological analysis by using transmission electron microscopy. All the authors contributed to discussions and reviewed the manuscript. All authors have read and agreed to the published version of the manuscript.

**Funding:** This research was funded by the Romanian Ministry of Research and Innovation (MCI) through the grant PN19-03 Core Program of NIMP (2020).

**Institutional Review Board Statement:** Not applicable.

**Informed Consent Statement:** Not applicable.

**Data Availability Statement:** Not applicable.

**Acknowledgments:** The authors acknowledge M Enculescu for the optical absorption measurements.

**Conflicts of Interest:** The authors declare no conflict of interest.

#### References

1. Zhong, T.; Goldner, P. Emerging rare-earth doped material platforms. *Nanophotonics* **2019**, *8*, 2003–2015. [[CrossRef](#)]
2. Escudero, A.; Becerro, A.I.; Carrillo-Carrión, C.; Núñez, N.O.; Zyuzin, M.V.; Laguna, M.; González-Mancebo, D.; Ocaña, M.; Parak, W.J. Rare earth based nanostructured materials: Synthesis, functionalization, properties and bioimaging and biosensing applications. *Nanophotonics* **2017**, *6*, 881–921. [[CrossRef](#)]
3. Stober, W.; Fink, A.; Bohn, E. Controlled growth of monodisperse silica spheres in the micron size range. *J. Colloid Interface Sci.* **1968**, *26*, 62–69. [[CrossRef](#)]
4. Van Hest, J.J.H.A.; Blab, G.A.; Gerritsen, H.C.; de Mello Donega, C.; Meijerink, A. Incorporation of Ln Doped  $\text{LaPO}_4$  Nanocrystals as Luminescent Markers in Silica Nanoparticles Nanoscale. *Res. Lett.* **2016**, *11*, 261.
5. Zhang, Y.; Lu, M. Labelling of silica microspheres with fluorescent lanthanide-doped  $\text{LaF}_3$  nanocrystals. *Nanotechnology* **2007**, *18*, 275603. [[CrossRef](#)]
6. Ando, M.; Li, C.; Yang, P.; Murase, N. Blue-Emitting Small Silica Particles Incorporating ZnSe-Based Nanocrystals Prepared by Reverse Micelle Method. *J. Biomed. Biotechnol.* **2007**, *2007*, 52971. [[CrossRef](#)]
7. Hreniak, D.; Jasiorski, M.; Hreniak, A.; Dudzinski, W.; Maruszewski, K.; Stręk, W. Preparation and Optical Properties of Submicron  $\text{SiO}_2$  Spheres Doped with  $\text{YAG:Nd}^{3+}$  Nanocrystallites. *J. Sol-Gel Sci. Technol.* **2003**, *26*, 971–976. [[CrossRef](#)]
8. Montini, T.; Melchionna, M.; Monai, M.; Fornasiero, P. Fundamentals and catalytic applications of  $\text{CeO}_2$ -based materials. *Chem. Rev.* **2016**, *116*, 5987–6041. [[CrossRef](#)]

9. Soni, S.; Chouhan, N.; Meena, R.K.; Kumar, S.; Dalela, B.; Mishra, M.; Meena, R.S.; Gupta, G.; Kumar, S.; Alvi, P.A.; et al. Electronic Structure and Room Temperature Ferromagnetism in Gd-doped Cerium Oxide Nanoparticles for Hydrogen Generation via Photocatalytic Water Splitting. *Glob. Chall.* **2019**, *3*, 1800090. [[CrossRef](#)]
10. Balestrieri, M.; Colis, S.; Gallart, M.; Schmerber, G.; Ziegler, M.; Gilliot, P.; Dinia, A. Photoluminescence properties of rare earth (Nd, Yb, Sm, Pr)-doped CeO<sub>2</sub> pellets prepared by solid-state reaction. *J. Mater. Chem. C* **2015**, *3*, 7014–7021. [[CrossRef](#)]
11. Liu, X.; Chen, S.; Wang, X. Synthesis and photoluminescence of CeO<sub>2</sub>:Eu<sup>3+</sup> phosphor powders. *J. Lumin.* **2007**, *127*, 650–654. [[CrossRef](#)]
12. Li, L.; Yang, H.K.; Moon, B.K.; Fu, Z.; Guo, C.; Jeong, J.H.; Yi, S.S.; Jang, K.; Lee, H.S. Photoluminescence Properties of CeO<sub>2</sub>:Eu<sup>3+</sup> Nanoparticles Synthesized by a Sol-Gel Method. *J. Phys. Chem. C* **2009**, *113*, 610–617. [[CrossRef](#)]
13. Yu, Y.; Chen, D.; Huang, P.; Lin, H.; Yang, A.; Wang, Y. Sensitization and protection of Eu<sup>3+</sup> luminescence by CeO<sub>2</sub> in nano-composite. *J. Alloys Compd.* **2012**, *513*, 626–629. [[CrossRef](#)]
14. D'Achille, A.E.; Wallace, R.M.; Coffey, J.L. Morphology-dependent fluorescence of europium-doped cerium oxide nanomaterials. *Nanoscale Adv.* **2021**, *3*, 3563–3572. [[CrossRef](#)]
15. Ackland, K.; Coey, J.M.D. Room temperature magnetism in CeO<sub>2</sub>—A review. *Phys. Rep.* **2018**, *746*, 1–39. [[CrossRef](#)]
16. Jiraskova, Y.; Bursik, J.; Janos, P.; Lunacek, J.; Chrobak, A.; Zivotsky, O. Effect of Iron Impurities on Magnetic Properties of Nanosized CeO<sub>2</sub> and Ce-Based Compounds. *Metals* **2019**, *9*, 222. [[CrossRef](#)]
17. Dimri, M.C.; Khanduri, H.; Kooskora, H.; Subbi, J.; Heinmaa, I.; Mere, A.; Krustok, J.; Stern, R. Ferromagnetism in rare earth doped cerium oxide bulk samples. *Phys. Status Solidi A* **2012**, *209*, 353–358. [[CrossRef](#)]
18. Kolodiaznyy, T.; Sakurai, H.; Belik, A.A.; Gornostaeva, O.V. Unusual lattice evolution and magnetochemistry of Nb doped CeO<sub>2</sub>. *Acta Mater.* **2016**, *113*, 116–123. [[CrossRef](#)]
19. Phoka, S.; Laokul, P.; Swatsitang, E.; Promarak, V.; Seraphinc, S.; Maensiri, S. Synthesis, structural and optical properties of CeO<sub>2</sub> nanoparticles synthesized by a simple polyvinyl pyrrolidone (PVP) solution route. *Mater. Chem. Phys.* **2009**, *115*, 423–428. [[CrossRef](#)]
20. Rietveld, H.M. A profile refinement method for nuclear and magnetic structures. *J. Appl. Cryst.* **1969**, *2*, 65–71. [[CrossRef](#)]
21. Lutterotti, L.; Matthies, S.; Wenk, H.-R. MAUD (Material Analysis Using Diffraction): A user friendly Java program for Rietveld Texture Analysis and more. In Proceedings of the Twelfth International Conference on Textures of Materials (ICOTOM-12), Montreal, QC, Canada, 9–13 August 1999; Volume 1, p. 1599.
22. ICDD. *Powder Diffraction File (PDF-4+ 2018 Software 4.18.0.2)*; International Centre for Diffraction Data: Newtown Square, PA, USA, 2011.
23. Binnemans, K.; Görller-Walrand, C.J. Application of the Eu<sup>3+</sup> ion for site symmetry determination. *J. Rare Earths* **1996**, *14*, 173–180.
24. Li, L.; Zhang, S.Y. Dependence of Charge Transfer Energy on Crystal Structure and Composition in Eu<sup>3+</sup>-Doped Compounds. *J. Phys. Chem. B* **2006**, *110*, 21438–21443. [[CrossRef](#)] [[PubMed](#)]
25. Fujihara, S.; Oikawa, M. Structure and luminescent properties of CeO<sub>2</sub>: Rare earth (RE = Eu<sup>3+</sup> and Sm<sup>3+</sup>) thin films. *J. Appl. Phys.* **2004**, *95*, 8002–8006. [[CrossRef](#)]
26. Miguez, H.; Lopez, C.; Meseguer, F.; Blanco, A.; Vazquez, L.; Mayoral, R.; Ocana, M.; Fornes, V.; Mifsud, A. Photonic crystal properties of packed submicrometric SiO<sub>2</sub> spheres. *Appl. Phys. Lett.* **1997**, *71*, 1148–1150. [[CrossRef](#)]
27. Sinitskii, A.S.; Knoko, A.V.; Tretyakov, Y.D. Silica photonic crystals: Synthesis and optical properties. *Solid State Ionics* **2004**, *172*, 477–479. [[CrossRef](#)]
28. Coey, M.; Ackland, K.; Venkatesan, M.; Sen, S. Collective magnetic response of CeO<sub>2</sub> nanoparticles. *Nat. Phys.* **2016**, *12*, 694–699. [[CrossRef](#)]